Facile preparation of p-CuO and p-CuO/n-CuWO$_4$ junction thin films and their photoelectrochemical properties

Jin You Zheng, Guang Song, Chang Woo Kim, Young Soo Kang*

Korea Center of Artificial Photosynthesis, Department of Chemistry, Sogang University, Seoul 121-742, Republic of Korea

ARTICLE INFO

ABSTRACT

CuO/CuWO$_4$ p–n junction thin films were prepared by using electrodeposited Cu films with an acidic cupric lactate system (pH $\leq$ 5). The photoelectrochemical properties of CuO and CuWO$_4$–CuO films were studied by photoresponse and current–potential characteristics under 1 sun illumination. The photocurrent of CuO films prepared by annealing Cu films electrodeposited at pH 5 is about 0.6 mA/cm^2 at -0.6 V vs Ag/AgCl. Both p-type and n-type behaviors occurred on CuO–CuWO$_4$ film in the potential range from 0.8 V to -0.6 V vs Ag/AgCl. The photoelectrochemical photocurrent switching (PEPS) effect was observed in the case of p-CuO/n-CuWO$_4$ heterojunction and the photocurrent switching potential is +0.33 V vs Ag/AgCl.

© 2012 Elsevier Ltd. All rights reserved.

1. Introduction

Cupric oxide, CuO, is a typically p-type semiconductor highly desirable for use in solar energy conversion because its narrow band gap (varies from 1.3 to 1.7 eV [1]) allows for utilizing a wide range of the solar energy spectrum. For solar water splitting, CuO has favorable energy band positions corresponding to Eg = 1.6 eV [1b], with the conduction band lying about 0.3 V more negative than the H$_2$ evolution potential and the valence band just covering the O$_2$ evolution potential in Fig. 1 [2]. The p-CuO photocathode can drive half of the water splitting reaction for H$_2$; another n-type photocathode or external bias is required for water oxidation to obtain O$_2$. However, the main disadvantage of CuO photocathode for water reduction is its instability in aqueous solution, because the redox potentials for the reduction and oxidation of copper oxide lie within the bandgap (as shown in Fig. 1) [3]. In the water splitting process, the CuO will become Cu$_2$O followed by Cu$_2$O reduction to Cu. In case of CuO instability in water under light illumination, the protective layer is required to stabilize the surface.

The photoelectrochemical photocurrent switching (PEPS) effect [4] has become a field of intensive study for numerous research groups. This unique effect can be utilized for nanoscale switching and information processing; furthermore, it can serve as an interface between molecular information processing and macroscopic electronics [5]. It can make use of both optical and electrical signals. This effect can be defined as switching of photocurrent polarity on changes in photoelectrode potential and/or incident light wavelength. The PEPS effect was observed in the case of n-TiO$_2$-N/p-CuI, n-CdS/p-CdTe, n-BiVO$_4$/p-Co$_3$O$_4$ and n-BiVO$_4$/p-CuO heterojunction composites [6].

Yourey et al. [7] reported that CuWO$_4$ obtained by electrodeposition is an n-type semiconductor with indirect band gap of 2.25 eV, 0.45 eV smaller than the gap of WO$_3$ as shown in Fig. 1. Compared to WO$_3$, CuWO$_4$ is more stable for the O$_2$-evolution half reaction of water splitting in aqueous electrolytes at pH 7. Recently, Chang et al. [8] also prepared co-sputtered polycrystalline CuWO$_4$ thin film with band gap of 2.25 eV for water splitting. It is possible to fabricate the effective p–n junction between CuO and CuWO$_4$ for enhanced charge separation according to the conduction and valence band positions of CuO and CuWO$_4$ as shown in Fig. 1. In this paper, p-CuO/n-CuWO$_4$ films were formed by spin coating the peroxytungstate precursor [9] on CuO films and the PEPS effect was observed in the case of p-CuO/n-CuWO$_4$ heterojunction. The preparation, characterization, and photoelectrochemical properties of p-CuO and p-CuO/n-CuWO$_4$ electrodes were investigated.

2. Experimental

2.1. Preparation of Cu, CuO and CuWO$_4$–CuO films

Cu was electrodeposited in a conventional three-electrode cell system using a potentiostat PL-9. The commercial indium-doped

---

* Corresponding author. Tel.: +82 2 705 8882; fax: +82 2 701 0967.
 *E-mail address:* yskang@sogang.ac.kr (Y.S. Kang).
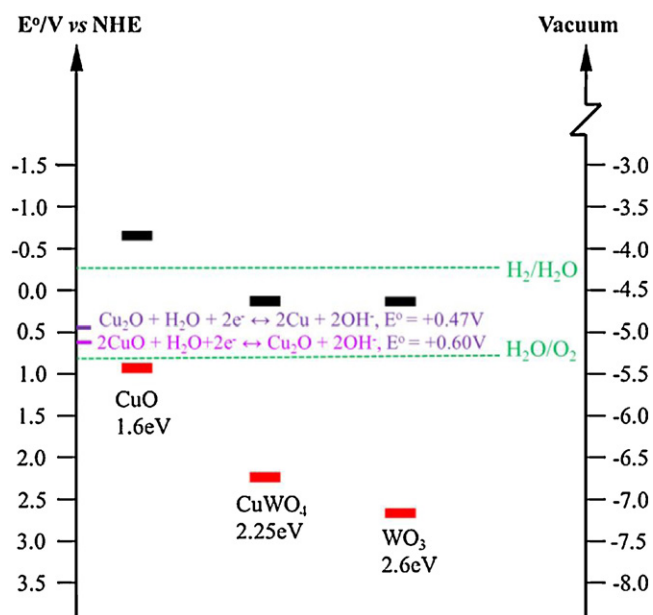
Fig. 1. Conduction band and valence band positions of CuO, CuWO$_4$ and WO$_3$ semiconductor photocatalysts relative to energy levels in contact with water vapor. The redox potentials H$_2$O splitting reactions at pH = 7 with respect to the normal hydrogen electrode (NHE) or vacuum.

Fig. 2. Schematic diagram showing the preparation process of Cu/ITO, CuO/ITO and CuWO$_4$–CuO/ITO films.

tin oxide (ITO) (film thickness 200 nm, resistance ≤10 Ω/□) glass was used as the working electrode. The ITO was dipped into the electrolyte solution and the immerged area was 0.8 cm^2. A coiled platinum wire and Ag/AgCl in 3 M KCl electrode were used as counter and reference electrode. All potentials reported in this work were measured with respect to Ag/AgCl electrode.

Cu films were deposited from the aqueous solution I containing 0.1 M Cu(NO$_3$)$_2$·2.5H$_2$O (Aldrich, 99.99+%) and 3 M lactic acid (Kanto, 85.0–92.0% solution in water) with different pH at −0.4 V vs Ag/AgCl for 30 min without stirring under ambient at 24 °C. The pH was adjusted by adding 4 M NaOH (Junsei, >96%). CuO films were obtained by annealing Cu films under air at 500 °C for 2 h (heating speed 2 °C/min) in the furnace. CuWO$_4$ layer was deposited on CuO films by spin coating (1500 rpm for 20 s) of the solution II [9], prepared by dissolving 1.25 g H$_2$WO$_4$ (Aldrich, ≥99.0%) and 0.5 g poly(vinyl alcohol) (PVA) (Aldrich, 99+%) in 10 mL 35 wt % H$_2$O$_2$ (Junsei, 35%), followed by annealing at 500 °C for 2 h in air. All chemicals were used without further purification.

2.2. Characterization

X-ray diffraction (XRD, Rigaku miniFlex-II desktop, Cu Kα) patterns and selected area electron diffraction (SAED, JEOL JEM-2100 F) pattern were used to check crystallinity and crystal structure of the deposits. Surface and cross-sectional morphologies of the films were obtained using a Hitachi Horiba S-4300 scanning electron microscope (SEM) operated at 20 kV. Photoelectrochemical measurements were conducted with potentiostat PL-9 in a conventional three-electrode system in a V-style with quartz window cell at room temperature under 1 sun (Asahi HAL-320, 100 mW/cm^2) illumination [10], employing a Pt foil and an Ag/AgCl electrode as counter and reference electrode, respectively. Photocurrent-potential was measured using linear sweep voltammogram (LSV) with a scan rate of 10 mV/s under a continuous or chopped light .0.5 M Na$_2$SO$_4$ (pH 6.3) was used as electrolyte solution. Photoresponses were measured by using chronoamperometry method at constant potential of −0.6 V vs Ag/AgCl ($E_{Ag/AgCl} = E_{RHE} - 0.0591 \times pH - 0.1976$ V, E_{2H+/H_2} (vs Ag/AgCl) ≈ −0.6 V).
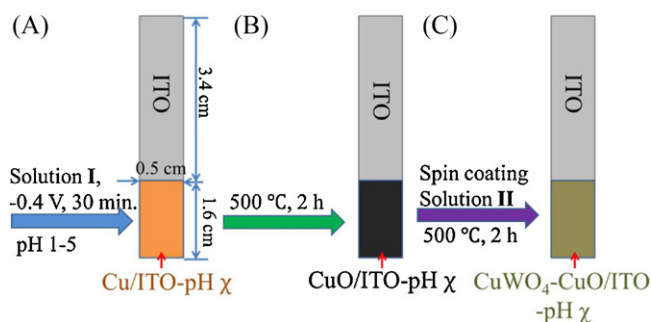
3. Results and discussion

The preparation of CuWO$_4$–CuO/ITO films by three steps, as shown in Fig. 2: (A) Cu/ITO-pH χ (χ = 1.2, 3, 5): room-temperature electrodeposition of Cu films in solution I containing 0.1 M Cu(NO$_3$)$_2$·2.5H$_2$O and 3 M lactic acid with different pH χ at −0.4 V vs Ag/AgCl for 30 min. (B) CuO/ITO-pH χ: annealing Cu films which were obtained at pH χ under air atmosphere at 500 °C for 2 h. (C) CuWO$_4$–CuO/ITO-pH χ: CuO combined with CuWO$_4$ by spin coating of solution II, followed by 500 °C anneal for 2 h in air. The basic cupric lactate system is a common solution system to form Cu$_2$O film on conductive substrates by electrochemical deposition [11–13]. However, few researchers have studied the synthesis of Cu film by this kind of cupric lactate system at acidic conditions. The lactic acids in the solution were complexed with free Cu^{2+} ions in solution to form Cu(CH$_3$CHOHCOO)$_2$ [12]. The lactate ions were used to stabilize Cu^{2+} ions by complexation [13].

SEM images of Cu films are shown in Fig. 3A. At pH = 1.2, the particles are irregular and there are no small grains on the surface. The particle surface is much smoother compared with those obtained at pH = 3 and 5. At pH = 3, the flower-like Cu particles are composed of triangular nanoplates with a thickness of 80 nm. The Cu particles are formed by many small grains; some grains with sharp tips appeared at pH = 5. The SAED pattern of Cu particles obtained at pH = 1.2 in Fig. 3A (a)-2 indicates that the Cu particles are polycrystal. In the solution, there are two chemical equilibria as following:

$$CH_3CHOHCOOH \leftrightarrow CH_3CHOHCOO^- + H^+$$

$$Cu^{2+} + 2CH_3CHOHCOO^- \leftrightarrow Cu(CH_3CHOHCOO)_2$$
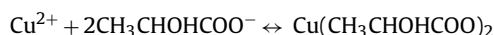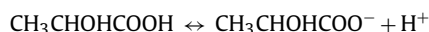
Therefore the concentration of effective Cu^{2+} ([Cu^{2+}]) is significantly pH-dependent and [Cu^{2+}]$_{pH=1.2}$ > [Cu^{2+}]$_{pH=3}$ > [Cu^{2+}]$_{pH=5}$. The ratios of mass-transport rate and crystal growth rate are distinct under different pH conditions. This is a possible reason that different morphologies can be formed at different pH levels.

XRD patterns in Fig. 4 indicate that the as-prepared Cu films and post-annealing at 500 °C for 2 h films are pure face-centered cubic-phase copper (JCPDS 65-9026) and pure monoclinic phase CuO (JCPDS 45-0937), respectively. SEM images of CuO films are shown in Fig. 3B. It can be seen that CuO/ITO-pH 1.2 film has two layers. The top layer is composed of CuO nanowires (NWs) with average length of 7 μm and diameter of 100 nm. The bottom layer is bulk CuO with hollows in the bottom and a thickness of about 8 μm. CuO/ITO-pH 3 film has lower coverage density and shorter CuO NWs. The bulk CuO with hollows in the center is about 1.7 μm and some protuberances appear in the surface. Especially, the CuO/ITO-pH 5 film has more apparent protuberances with vacant bottom and without CuO NWs on bulk CuO. The formation of hollows at the interface can be attributed to the existence of interspaces between Cu
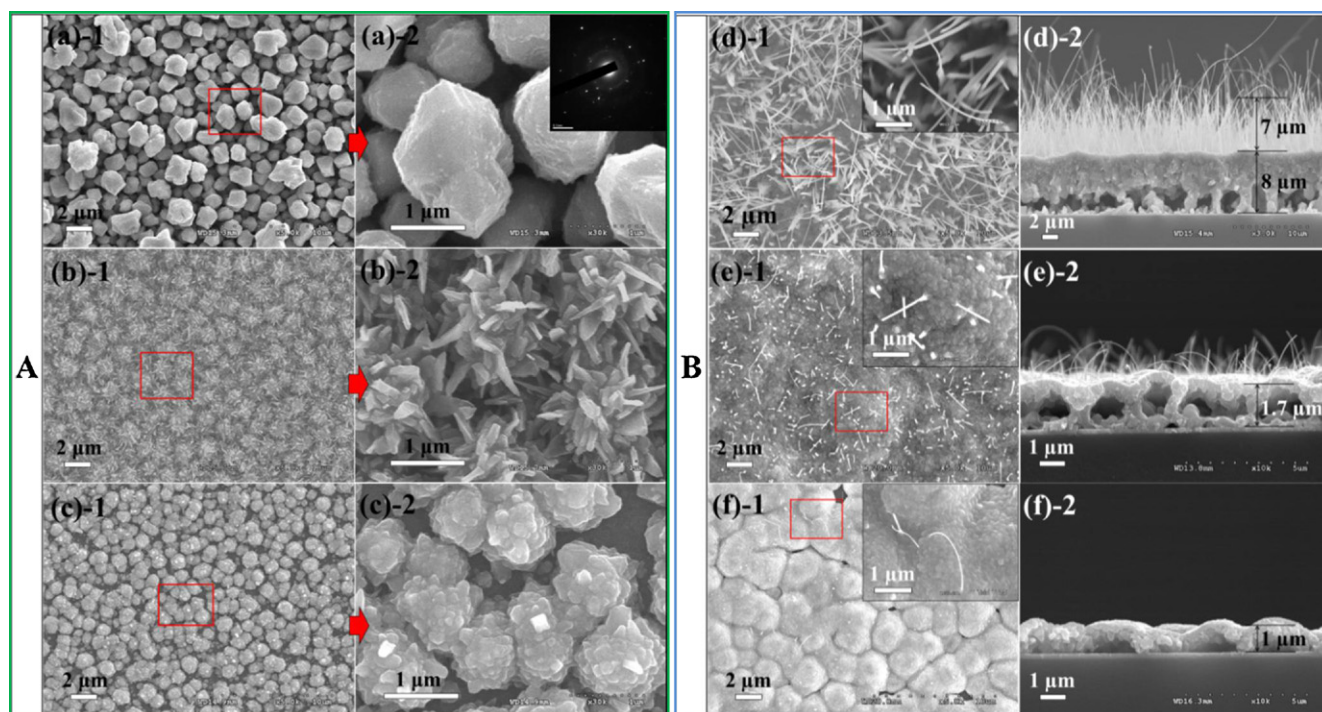
Fig. 3. SEM images of (A) as-electrodeposited Cu films and (B) CuO films obtained by Cu films thermal oxidation. (a) Cu/ITO-pH 1.2, (b) Cu/ITO-pH 3, (c) Cu/ITO-pH 5, (d) CuO/ITO-pH 1.2, (e) CuO/ITO-pH 3, and (f) CuO/ITO-pH 5. Inset of A(a)-2 is the SAED pattern of Cu particle for the sample obtained at pH = 1.2. Insets of (d)-1, (e)-1 and (f)-1 are the high-magnification SEM images corresponding to red rectangles. (d)-2, (e)-2 and (f)-2 are the cross-section SEM images.

particles. Another reason is that the effect of annealing Cu films at high temperatures allows mass transport of either individual Cu atoms or small clusters across the surface in which larger clusters could be formed out of smaller clusters in a process analogous to Ostwald ripening [14]. To compare the stability of connecting CuO film with ITO substrate and CuO with Cu substrate, Cu foil (99.98%, 0.5 mm thickness) was annealed directly with the same annealing process as Cu/ITO converted to CuO/ITO. It indicates that the CuO NWs grow on the surface of CuO/Cu$_2$O/Cu multilayer structure; similar results have been previously noted [15]. However, the black CuO film was easily peeled off from the Cu substrate in the cooling process. In contrast, the stability of connecting CuO film with ITO is very good.

Fig. 4. XRD patterns of as-prepared Cu films obtained at different pH (a) pH = 5, (b) pH = 3 and (c) pH = 1.2; and the CuO films (d), (e) and (f) obtained by annealing the Cu films at 500 °C for 2 h, respectively.

The photocurrent of copper oxide is induced by the creation of electron–hole pairs and the subsequent increase of minority carriers of electrons for p-type semiconductors under illumination [16]. Fig. 5A shows the current–potential characteristics of CuO films under 1 sun illumination (Asahi HAL-320 Sun simulator, 100 mW/cm^2) for the first scanning. As the potential sweeps to the negative direction from +0.7 V to −0.7 V vs Ag/AgCl, cathodic photocurrents are observed. The photocurrent of CuO electrodes is in order of CuO/ITO-pH 1.2 < CuO/ITO-pH 3 < CuO/ITO-pH 5, the opposite order with CuO films thickness. So the largest photocurrent for the CuO/ITO-pH 5 electrode might be due to its thinnest CuO film, which has the shortest charge carrier transport length thus reducing the rate of effective recombination of electron–hole pairs. Fig. 5B shows a great initial cathodic photocurrent spike occurs before a steep decay to a steady-state photocurrent. The reasons of decay are attributed to the significant electron–hole recombination at instantaneous time or corrosive effects through all checking time. The photocurrents after 150 s photoresponse are 0.29, 0.48 and 0.60 mA/cm^2 at −0.6 V vs Ag/AgCl, corresponding to CuO/ITO pH 1.2, 3 and 5, respectively.

CuWO$_4$–CuO/ITO electrode was prepared by spin coating of the acidic peroxytungstic acid precursor (representing with H$_2$W$_2$O$_{11}$ [7,17]) on CuO film and followed by calcination. The possible reactions were existed in annealing process as following equations.

$$H_2W_2O_{11}(l) + 2CuO(s) \rightarrow 2CuWO_6(s) + H_2O(g)$$

$$CuWO_6(s) \rightarrow CuWO_4(s) + O_2(g)$$
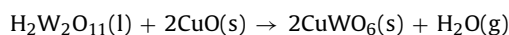
The redundant WO$_3$ in the film can be ignored. The reasons are as following explanations. First, the thickness of CuWO$_4$ film is very thin, about 200 nm; and the XRD in Fig. 6(C) show only CuWO$_4$ and CuO. Second, considering components of the acidic peroxytungstic acid precursor, there are H$_2$W$_2$O$_{11}$ and residual H$_2$O$_2$; they are acidic and oxidative, and very easy to react with CuO to
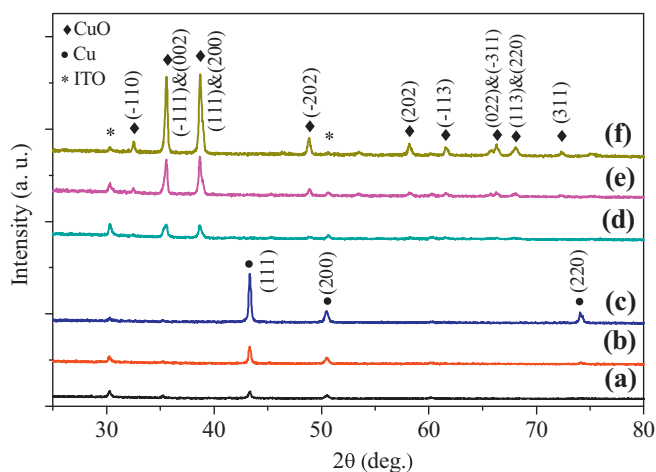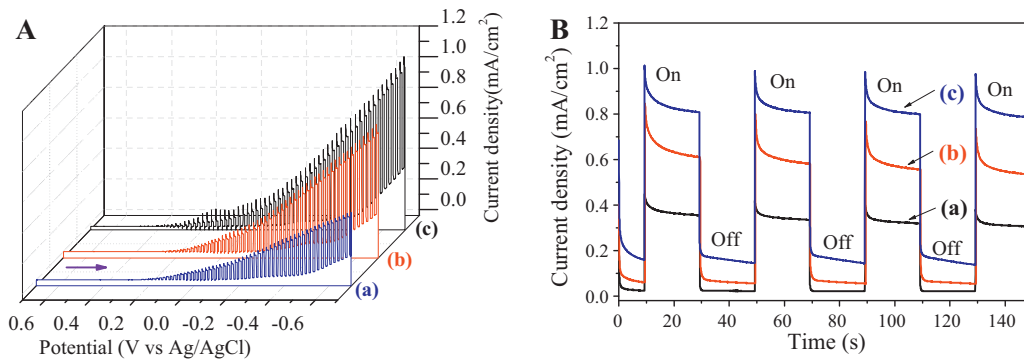
Fig. 5. (A) Current–potential characteristics of CuO films under 1 sun illumination and (B) photoresponse at −0.6 V vs Ag/AgCl for the CuO films. (a) CuO/ITO-pH 1.2, (b) CuO/ITO-pH 3, and (c) CuO/ITO-pH 5. Arrow in (A) indicates the initial direction of potential sweep.

form Cu^{2+} or $CuWO_6$ even before annealing process. Fig. 6(A) and (B) shows the top-view and cross-section of SEM images exposing the layers of $CuWO_4$–CuO/ITO-pH 5 electrode. The XRD pattern in Fig. 6(C) was similar to one previously shown [7]; the upper film is triclinic $CuWO_4$ from JCPDS 72-0616. It was an intentionally covered $CuWO_4$ layer (~200 nm thickness) to use it as a physical barrier to minimize direct contact between CuO and the electrolyte, which may alleviate the aforementioned reductive decomposition problem. Fig. 6(D) shows that the onset potential for photocurrent of the bare CuO/ITO-pH 5 is +0.43 V vs Ag/AgCl. The cathodic photocurrent of the $CuWO_4$–CuO/ITO electrode gradually decreases as the applied potential is swept to the positive direction and is converted to anodic photocurrent at +0.33 V vs Ag/AgCl. As the potential continually increases, the anodic photocurrent also increases. The conversion of p-type behavior to n-type behavior happens at +0.33 V vs Ag/AgCl. The deposition of an n-type $CuWO_4$ later on top of a p-type CuO should lead to the formation of a p–n junction. For this reason the onset potentials of CuO and $CuWO_4$–CuO are different. The cathodic photocurrents should

therefore correspond to a condition in which electron holes are separated at the p–n junction, with electrons moving towards the electrolyte and holes moving towards the ITO. The anodic photocurrent should correspond to electron hole separation at the Schottky barrier between the electrolyte and the $CuWO_4$. The photocurrent of $CuWO_4$–CuO/ITO is 0.49 mA/cm² at −0.6 V vs Ag/AgCl. Since the resistance of ITO can increase to four times after annealing 500 °C for 2 h, a possible explanation as to why the photocurrent of CuO decreased after combination with $CuWO_4$ is that the resistance of $CuWO_4$–CuO/ITO-pH 5 is greater than the resistance of CuO/ITO-pH 5. The onset potential for dark current of $CuWO_4$–CuO/ITO electrode shifts slightly to the positive direction and the dark current of $CuWO_4$–CuO/ITO is higher than CuO/ITO in the range from −0.2 V to −0.7 V vs Ag/AgCl. The plausible explanations for these cases are that H_2 evolution or reduction of O_2 to O_2^- [6c] become easier after combined with $CuWO_4$; another possible excuse is caused by the inherent property of $CuWO_4$ film, which is that the cathodic dark current increases abruptly after the potential scanning lower than approximately −0.2 V vs Ag/AgCl [7]. However, the photocurrent
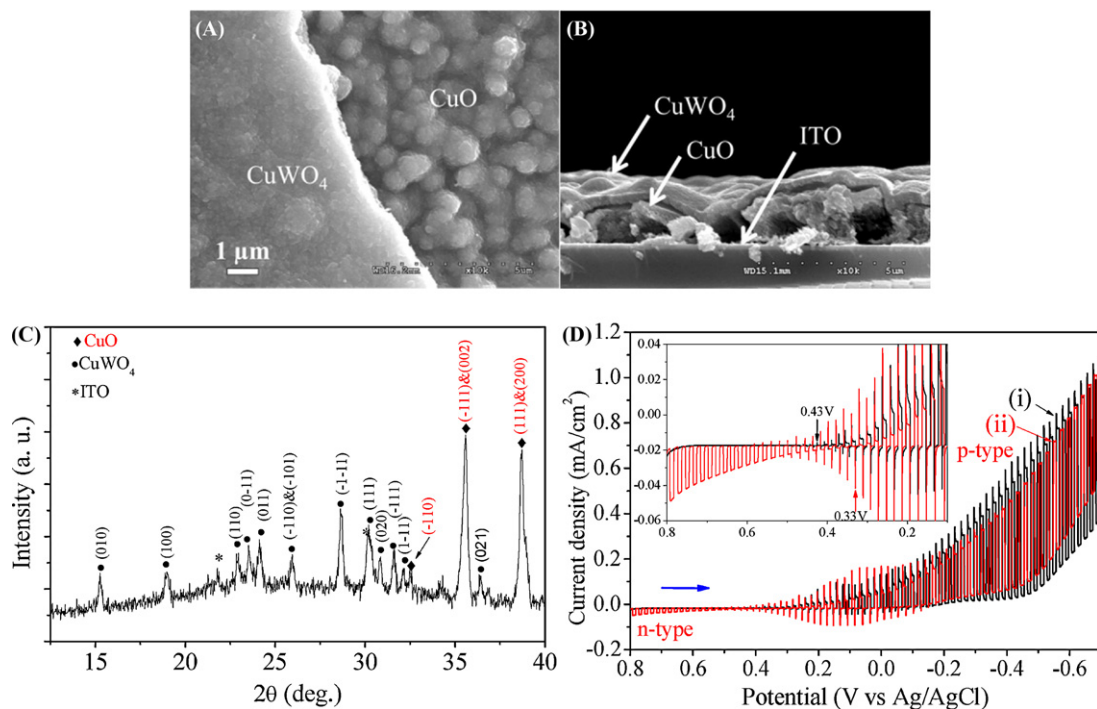
Fig. 6. SEM images (A) top-view, (B) cross-section, (C) XRD pattern and (D) current–potential characteristics of $CuWO_4$–CuO/ITO-pH 5 electrode with chopped 1 sun; (i) (black color) CuO/ITO-pH 5 and (ii) (red color) $CuWO_4$–CuO/ITO-pH 5 film. Inset: the high-magnification potential range from 0.8 V to 0.1 V vs Ag/AgCl. Arrow (blue color) in (D) indicates the initial direction of potential sweep. (For interpretation of the references to color in this figure legend, the reader is referred to the web version of this article.)

of CuWO$_4$–CuO/ITO, at the potential range from −0.4 V to −0.7 V vs Ag/AgCl, has lower recombination of electron–hole pairs since there are no great initial cathodic photocurrent spikes.

4. Conclusions

In conclusion, the pure Cu films with different morphologies were synthesized by electrochemical deposition in an acidic cupric lactate system (pH ≤ 5). After thermal oxidation treatment, the Cu films were oxidized to CuO films with hollows and nanowires. The photocurrent of CuO/ITO-pH 5 is 0.6 mA/cm^2 at −0.6 V vs Ag/AgCl. After spin-coating and thermal treatment, the CuWO$_4$ layer with 200 nm thickness was formed on the CuO surface. Both p-type and n-type behaviors occurred in the potential range from 0.8 V to −0.6 V vs Ag/AgCl and the photocurrent switching potential is +0.33 V vs Ag/AgCl.

Acknowledgements

References

[1] (a) F.P. Koffyberg, F.A. Benko, J. Appl. Phys. 53 (1982) 1173;
(b) K. Nakaoka, J. Ueyama, K.J. Ogura, J. Electrochem. Soc 151 (2004) C661.
[2] S.C. Roy, O.K. Varghese, M. Paulose, C.A. Grimes, ACS Nano 4 (2010) 1259.
[3] A. Paracchino, V. Laporte, K. Sivula, M. Gratzel, E. Thimsen, Nat. Mater. 10 (2011) 456.
[4] K. Szaciłowski, W. Macyk, Chimia 61 (2007) 831.
[5] S. Gaweda, A. Podborska, W. Macyka, K. Szaciłowski, Nanoscale 1 (2009) 299.
[6] (a) R. Beranek, H. Kisch, Angew. Chem. Int. Ed. 47 (2008) 1320;
(b) G. Agostinelli, E.D. Dunlop, Thin Solid Films 448 (2003) 431;
(c) M. Long, R. Beranek, W. Cai, H. Kisch, Electrochim. Acta 53 (2008) 4621.
[7] J.E. Yourey, B.M. Bartlett, J. Mater. Chem. 21 (2011) 7651.
[8] Y. Chang, A. Braun, A. Deangelis, J. Kaneshiro, N. Gaillard, J. Phys. Chem. C 115 (2011) 25490.
[9] J.Z. Su, X.J. Feng, J.D. Sloppy, L.J. Guo, C.A. Grimes, Nano Lett. 11 (2011) 203.
[10] H.G. Cha, J. Song, H.S. Kim, W.S. Shin, K.B. Yoon, Y.S. Kang, Chem. Commun. 47 (2011) 2411.
[11] (a) M. Izaki, K. Mizuno, T. Shinagawa, M. Inaba, A. Tasakab, J. Electrochem. Soc. 153 (2006) C668;
(b) C.M. McShane, W.P. Siripala, K.S. Choi, J. Phys. Chem. Lett. 1 (2010) 2666.
[12] A.E. Rakhshani, J. Varghese, Sol. Energy Mater. 15 (1987) 237.
[13] T.D. Golden, M.K. Shumsky, Y.C. Zhou, R.A. VanderWerf, R.A. Van Leeuwen, J.A. Switzer, Chem. Mater. 8 (1996) 2449.
[14] (a) U. Diebold, J.M. Pan, T.E. Madey, Phys. Rev. B 47 (1993) 3868;
(b) J.D. Carey, L.L. Ong, S.R.P. Silva, Nanotechnology 14 (2003) 1223.
[15] L.S. Huang, S.G. Yang, T. Li, B.X. Gu, Y.W. Du, Y.N. Lu, S.Z. Shi, J. Cryst. Growth 260 (2004) 130.
[16] P.E. de Jongh, D. Vanmaekelbergh, J.J. Kelly, J. Electrochem. Soc. 147 (2000) 486.
[17] E. Lassner, W.D. Schubert, Tungsten: Properties, Chemistry, Technology of the Element, Alloys, and Chemical Compounds, Springer, 1999, p. 160.